Observation of transverse modes in a microchip laser with combined gain and index guiding

N. J. van Druten*

Huygens Laboratory, Universiteit Leiden, P.O. Box 9504, Leiden, The Netherlands, and Department of Applied Physics, Delft University of Technology, Lorentzweg 1, 2628 CJ Delft, The Netherlands

S. S. R. Oemrawsingh, Y. Lien, C. Serrat,† M. P. van Exter, and J. P. Woerdman

Huygens Laboratory, Universiteit Leiden, P.O. Box 9504, Leiden, The Netherlands

Received February 27, 2001; revised manuscript received May 31, 2001

The transverse-mode profiles for a plano–concave Nd:YVO_4 microchip laser near threshold are examined, both experimentally and theoretically, and in both the near and the far field. We study in particular the transition from dominant quadratic index guiding to dominant gain guiding. The modal profiles change dramatically in this transition, and the agreement between experiment and the theoretical model is excellent. © 2001 Optical Society of America

OCIS codes: 140.0140, 140.3530, 140.3410, 140.5680, 140.4780, 230.7370.

1. INTRODUCTION

Microchip lasers[1] are interesting devices from both a practical[2] and a fundamental[3,4] point of view. They typically consist of a thin (approximately millimeter) rare-earth-doped laser crystal; the usual dopant is Nd^{3+}. The crystal has a dielectric coating on both faces to form a complete plane parallel cavity, longitudinally pumped by a diode laser. Single-frequency operation is readily obtained in these lasers, and the monolithic cavity is beneficial to stable operation. They require little material, and their relatively simple design makes them good candidates for mass fabrication.

One of the aspects of these lasers that has received considerable attention is their transverse mode structure.[5–13] Because of the planar nature of the cavity, the transverse eigenmodes are determined not by mirror curvatures but rather by weaker, residual guiding effects such as gain guiding or thermal guiding. Thus the usual Laguerre– or Hermite–Gaussian transverse modes are not necessarily established in microchip lasers. In quasi-three-level (i.e., *not* Nd^{3+} based) lasers the inherent absorption in the unpumped regions of the laser crystal leads to a soft transverse gain aperture that typically dominates the guiding,[7] simplifying the description. In contrast, in four-level lasers (based on Nd^{3+}) the unpumped region can have very low absorption, and the situation is not so clear cut. In this case both thermal guiding[5] and gain guiding[9] have been observed as dominant mechanisms, but the transition region between the two has received very little attention so far.

An additional motivation to study the guiding mechanism is as follows. Lasers based on rare-earth-doped microchip crystals have already been used for a number of fundamental quantum-noise studies.[3,4,14] Of particular interest for so-called *excess* quantum noise[14–17] is the combination of conservative (e.g., thermal guiding, index guiding, or gain-related index guiding) and dissipative (e.g., aperture guiding, gain guiding) guiding mechanisms, because it is this combination that generally leads to highly nonorthogonal eigenmodes and hence to large excess quantum-noise factors.[15–17]

Motivated by these considerations, some of us recently investigated the theory of such a combination of guiding mechanisms[13] and found a highly varied transverse mode structure. Specifically, the combination of a quadratic index guide and a Gaussian gain guide was studied for a four-level laser system, with the waist size of the Gaussian gain being considerably smaller than the lasing-mode waist size that would result from the index guide alone. Although it may seem that this particular combination is one of many cases that could be studied, it is in fact a very common case for microchip lasers: The gain in these lasers is provided by a longitudinal pump whose transverse profile may usually be approximated as being Gaussian. Similarly, the index guide in microchip lasers is usually quadratic, as we now discuss in some more detail.

There are a number of possible origins for index guiding in microchip lasers, e.g., the use of concave mirrors, thermal lensing (temperature-induced change in refractive index), and thermal curvature of the crystal surface. When concave mirrors are used and the cavity is thin, the guiding provided by the mirrors can be treated as an effective quadratic index guide.[13] The thermal guiding mechanisms are typically much weaker, and these are often neglected compared with the gain-related guiding.[6,8,11] When thermal effects *are* considered, approxi-

mating the resulting weak index guide to the lowest nonvanishing order (i.e., as a quadratic guide) seems reasonable.[5,12]

Here we report the experimental observation of the rich mode structure predicted previously.[13] The experiment employs an external concave mirror and a titanium–sapphire pump beam as well-defined sources of the quadratic index guide and the Gaussian gain guide, respectively. The dependence on cavity detuning is studied, and both near-field and far-field mode profiles are shown. The observed transverse modes are significantly different from the usual Laguerre–Gaussian modes and exhibit several noteworthy features, such as conical emission[10] and the appearance of several rings in the far field in the absence of ring structure in the near field. A detailed comparison with an extended version of our previous theoretical model[13] is given. The theoretical model has been kept simple, e.g., the nonlinearities related to gain saturation (e.g., spatial hole burning) and the complicated temporal dynamics related to the slow inversion[4] have been neglected. Nevertheless, we find very good agreement with experiment over the full range of mode structures when the laser is operated close to threshold.

The outline of this paper is as follows. In Section 2 we present the theoretical model. Our previous model[13] is summarized and extended to include the effects of frequency detuning, in particular the dispersion of the inverted gain medium (gain-related index guiding). The latter will turn out to be highly relevant for a proper comparison with the experiments. The detuned operation is in fact quite natural for thin microchip lasers, and the consequences thereof for the guiding have been pointed out previously.[6,10–12] We illustrate the importance of the relative strength of the gain-related guiding and index guiding and emphasize the role of the mirror reflectivity in determining this relative strength. Next, in Section 3, we discuss the experimental setup and the precise experimental cavity configuration. The transverse mode profiles and their respective modal gains as obtained experimentally and theoretically are presented and compared in Section 4. This is followed by a discussion of the results in Section 5. Finally, we summarize and conclude in Section 6.

2. THEORETICAL MODEL

The model we use is based on the configuration schematically depicted in Fig. 1(a). We consider a cavity of length L, filled with a medium with a base refractive index n_0, having a parabolic index guide Δn_R and a Gaussian gain guide represented by a (complex-valued) refractive-index change Δn_g. The key simplification made here is that the gain is modeled as simple linear amplification (i.e., Δn is independent of intensity). Only the transverse spatial dependence of the gain is taken into account, while saturation and temporal dynamics of the gain medium (including spatial and temporal hole burning) are neglected. Thus the model is aimed at a laser operating close to threshold. The condition for lasing will be imposed by requiring that the lowest-loss transverse eigenmode has zero net loss after a full round trip. A discussion of the above approximations, and how they apply to our experimental setup, is provided in Section 5.

Because of the approximation of linear gain, we do not consider longitudinal spatial hole burning, and the standing-wave cavity of length L in Fig. 1(a) can be unfolded and treated as a waveguide of length $2L$, in which the optical wave travels in a single direction only. Our starting point is now the paraxial wave equation, which may be written in cylindrical coordinates $\mathbf{r} = (r, \phi, z)$ as

$$\left[\nabla_r^2 + 2k_z^2\left(\frac{\Delta\omega}{\omega_{\mathrm{at}}} + \frac{\Delta n}{n_0}\right)\right]u = -2ik_z\frac{\partial u}{\partial z}, \tag{1}$$

where

$$\nabla_r^2 = \frac{\partial^2}{\partial r^2} + \frac{1}{r}\frac{\partial}{\partial r} + \frac{1}{r^2}\frac{\partial^2}{\partial \phi^2} \tag{2}$$

is the usual transverse Laplacian. Here $u(\mathbf{r})$ is the (slowly varying) amplitude of the electric field component

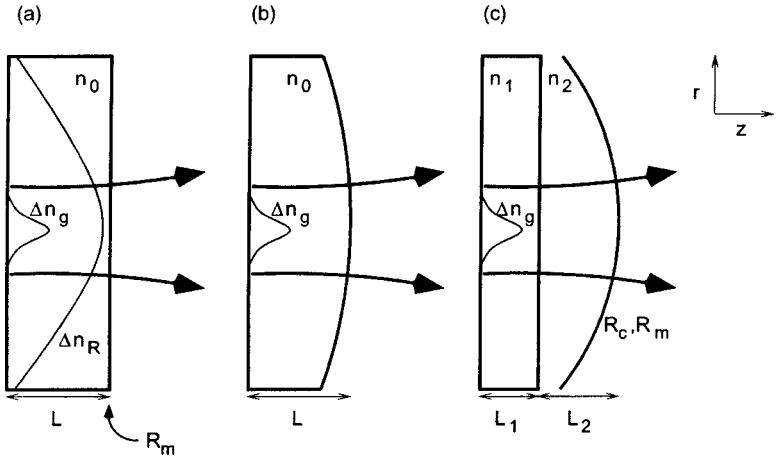

Fig. 1. (a) Cavity configuration considered in the theoretical model: a longitudinally homogeneous system of length L, with a transverse quadratic index guide Δn_R and a Gaussian gain guide Δn_g. The arrows in this figure indicate the output of the microchip laser through the end mirror with reflectivity R_m. Arrangements (b) and (c) are equivalent configurations[13] as long as the longitudinal variation of the mode profile may be neglected. (b) Monolithic cavity with a gain guide Δn_g and a curved surface. (c) Cavity configuration used in the experiments: a crystal gain medium with a transverse Gaussian gain profile and a separate concave mirror, with radius of curvature R_c and reflectivity R_m.

E of the electromagnetic field, a monochromatic wave at frequency ω and wave vector close to $k_z \equiv n_0\omega_{\mathrm{at}}/c$ in the $+z$ (longitudinal) direction, with a fixed polarization

$$E(\mathbf{r}) = u(\mathbf{r})\exp - i(\omega t - k_z z). \tag{3}$$

The detuning $\Delta\omega = \omega - \omega_{\mathrm{at}}$ refers to the reference frequency ω_{at} and the (complex-valued) guiding $\Delta n(\mathbf{r}) = n(\mathbf{r}) - n_0$ to the (real-valued) base refractive index n_0 of the medium in the absence of guiding. These have been included to first order only; i.e., we assume $\Delta\omega/\omega_{\mathrm{at}} \ll 1$ and $\Delta n(\mathbf{r})/n_0 \ll 1$, as is natural within the paraxial approximation.

The explicit form of the guiding we use throughout this paper is $\Delta n = \Delta n_R + \Delta n_g$, where

$$\Delta n_R(\mathbf{r}) = -\frac{2n_0 r^2}{k_z^2 w_0^4}, \tag{4}$$

$$\Delta n_g(r, \Delta\omega) = -\frac{c g(\mathbf{r}, \Delta\omega)}{2\omega_{\mathrm{at}}}, \tag{5}$$

with

$$g(r, \Delta\omega) = g_0 \exp(-2r^2/w_g^2)\frac{i - \Delta\omega/\gamma_{\mathrm{at}}}{1 + (\Delta\omega/\gamma_{\mathrm{at}})^2}. \tag{6}$$

Here Δn_R is the quadratic index guide, with a strength parameterized by w_0, the waist size of the Gaussian beam[18] that would be an eigenmode if this were the only guiding present. The gain guide $\Delta n_g(r, \Delta\omega)$ is a radial Gaussian with waist size w_g and peak gain per length g_0. It is a Lorentzian in frequency, as is appropriate for a homogeneously broadened gain medium,[18] with a FWHM (in radial frequency ω) of $2\gamma_{\mathrm{at}}$; the reference frequency ω_{at} has been fixed at the line center of the gain medium. The imaginary part of $g(r, \Delta\omega)$ represents the gain, while the real part represents the dispersion of the gain medium when detuned from resonance. The latter has been referred to as the gain-related index guide,[12] and we adopt that nomenclature here.

It will be convenient to rescale the transverse coordinate r to $\rho = r/w_0$. This transforms Eq. (1) into

$$\left[-\frac{1}{2}\nabla_\rho^2 + 2\rho^2 + z_0 g\right]u = 2iz_0\left[\frac{\partial u}{\partial z} - \frac{in_0\Delta\omega}{c}u\right], \tag{7}$$

with

$$\nabla_\rho^2 = \frac{\partial^2}{\partial\rho^2} + \frac{1}{\rho}\frac{\partial}{\partial\rho} + \frac{1}{\rho^2}\frac{\partial^2}{\partial\phi^2}, \tag{8}$$

the rescaled transverse Laplacian, and $z_0 = k_z w_0^2/2$, the Rayleigh range corresponding to the waist size w_0. The amplitude u is now considered a function of ρ instead of r. Because the guiding of Eqs. (4)–(6) has cylindrical symmetry, Eq. (1) is separable in cylindrical coordinates. In addition, since the gain is maximum on axis, higher-order angular momentum modes (having zero intensity on axis) will not be important close to laser threshold, and we can limit the analysis to the lowest-order angular momentum modes, eliminating the ϕ dependence.

The transverse eigenmodes of the laser are fully determined by the eigenfunctions of the left-hand side of Eq. (7), which in turn depend on $z_0 g$. The latter depends on three dimensionless parameters [cf. Eq. (6), inserting $r = \rho w_0$], namely, the on-axis gain per Rayleigh range $z_0 g_0$, the (rescaled) gain waist size w_g/w_0, and the scaled detuning $\Delta\omega/\gamma_{\mathrm{at}}$. For such an eigenfunction $u_\mu(\rho)$ with (dimensionless) eigenvalue μ, the z dependence follows directly from the right-hand side of Eq. (7), namely,

$$u_\mu(\rho, z) = u_\mu(\rho, 0)\exp[i(n_0\Delta\omega/c - \mu/2z_0)z]. \tag{9}$$

For a laser at threshold, we demand that the mode amplitude E_0 of the lowest-loss eigenmode reproduce after one round trip; i.e., taking into consideration the mirror intensity reflectivity R_m, we need

$$\sqrt{R_m}E_0(z + 2L) = E_0(z). \tag{10}$$

This results in a condition on the eigenvalue,

$$\mu = 2z_0\left(k_z + \frac{n_0\Delta\omega}{c} - \frac{\pi m}{L} - \frac{i}{4L}\ln R_m\right), \tag{11}$$

where m is the longitudinal mode index, an integer ($m \gg 1$). The imaginary part of the eigenvalue, $\mathrm{Im}\,\mu$, is thus fixed by the mirror reflectivity with the condition of being at threshold. The real part of the eigenvalue, $\mathrm{Re}\,\mu$, is dictated by the fact that the phase shift of the field during a round trip is a multiple of 2π.

We can tune this phase shift by adjusting the length of the cavity. By expanding the length L and the mode index m around convenient values of L_0 and m_0 chosen such that $k_z = \pi m_0/L_0$, i.e., such that a multiple of half-wavelengths fits into L_0, we obtain

$$\frac{2\Delta L}{\lambda_{\mathrm{at}}} = \left[-\frac{\Delta\omega}{\omega_{\mathrm{FSR}}} + \tilde{m} + \frac{L_0\,\mathrm{Re}\,\mu}{2\pi z_0}\right], \tag{12}$$

where $\Delta L = L - L_0$, $\tilde{m} = m - m_0$, and $\omega_{\mathrm{FSR}} = \pi c/n_0 L_0$ is the free spectral range of the cavity.

The straightforward approach to the eigenvalue problem of the left-hand side of Eq. (7) would be to specify the three parameters $z_0 g_0$, w_g/w_0, and $\Delta\omega/\gamma_{\mathrm{at}}$ and numerically find the eigenvalues μ and eigenfunctions $u_\mu(\rho)$. This is not efficient, however, because an experimental configuration will fix $\mathrm{Im}\,\mu$ and ΔL instead of g_0 and $\Delta\omega$. As an additional complication, fixing ΔL imposes a boundary condition on a combination of $\Delta\omega$ and $\mathrm{Re}\,\mu$ [cf. Eq. (12)], while $\mathrm{Re}\,\mu$ itself also depends on $\Delta\omega$. The parameter space of the eigenvalue equation would thus have to be searched for cases in which μ matches the boundary conditions imposed by Eq. (11).

Instead, we have adopted a slightly different procedure to find the transverse eigenmodes. First, a cavity configuration is chosen by specifying values for w_g/w_0 and $z_0\ln(R_m)/L_0$. This directly determines the required modal gain $\mathrm{Im}\,\mu$ [cf. Eq. (11)]. The eigenmodes at threshold can now be found numerically from Eq. (7) as a function of $\Delta\omega/\gamma_{\mathrm{at}}$ by allowing g_0 (instead of $\mathrm{Im}\,\mu$) and $\mathrm{Re}\,\mu$ to vary, subject to the boundary condition that $u(\rho)$ vanishes as $\rho \to \infty$. The resulting g_0 is proportional to the pump power needed to bring the mode to threshold, while $\mathrm{Re}\,\mu$ can be used together with Eq. (12) to find the length at which the mode is resonant. Taken together, this allows us to plot threshold pump powers and mode profiles as a function of cavity length for that particular cavity configuration. For each solution the near-field intensity pro-

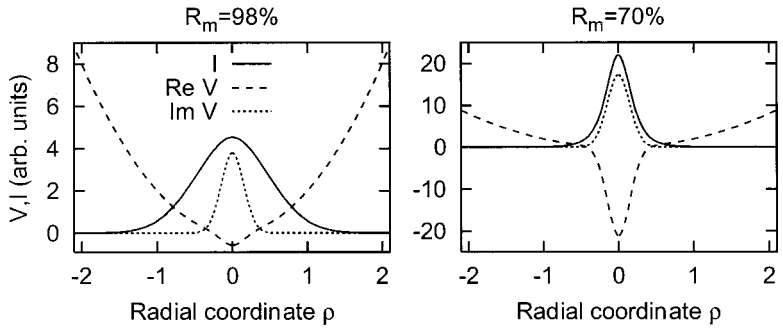

Fig. 2. Transverse profile of the real (dashed curve) and imaginary (dotted curve) part of the guiding potential $V \propto \Delta n$, for $w_g/w_0 = 0.3$, and for the detuning $\Delta\omega$, where the modal gain needed to reach threshold is lowest. The transverse mode profile of the lowest-loss eigenmode (solid curve, with the vertical scale adjusted in each plot), is shown for comparison. Left, $\mathrm{Im}\,\mu = 0.36$ (corresponding to $R_m = 98\%$ in the experiment); the parabolic part (the mirror curvature) of the real index guide dominates. Right, $\mathrm{Im}\,\mu = 6.3$ ($R_m = 70\%$); the Gaussian guide dominates, as it confines the mode to a region where the parabolic index guide is relatively small. Note the difference in vertical scale (for V) between the two plots.

file $I(r)$ is given simply by $I(r) \propto |u(\rho)|^2$ (with $\rho = r/w_0$), while the far-field profile $I(\theta)$ is obtained by numerically performing the conversion integral

$$I(\theta) \propto \left| \int_0^\infty u(\rho) J_0(k_z w_0 \rho \theta) \mathrm{d}\rho \right|^2, \qquad (13)$$

where J_0 is the zeroth-order Bessel function of the first kind.

The above treatment extends our previous model[13] in two ways: (i) The gain-related index guide that occurs when detuning away from gain maximum is included [cf. the dependence on $\Delta\omega$ in Eq. (6)]; (ii) the round trip resonance condition is explicitly included, by means of Eq. (12). Note that these two extensions are closely related, since a fixed cavity length will generally impose a detuning away from gain maximum on the eigenmodes. The current model is similar to the models used previously by others to describe gain (-related) guiding in rare-earth microchip lasers,[6,8,11] the difference being that we have included a parabolic index guide (in addition to the Gaussian radial variation in gain), while previous work[6,8,11] included the saturation of the gain medium instead (and in some cases other radial gain distributions).

One of the key points, as was pointed out before,[13] is that around laser threshold the relative importance of the gain guiding and the parabolic index guiding is set mainly by the mirror reflectivity. This can be readily understood as follows. The mirror reflectivity (or, more generally, the overall round-trip loss) directly determines the modal gain that is needed to reach laser threshold [this condition is explicit in the imaginary part of Eq. (11)]. For high mirror reflectivities little gain is needed, resulting in only weak gain-related guiding, so that the parabolic index guide dominates. In contrast, for low mirror reflectivities high modal gain is needed, and the gain-related guiding will dominate the parabolic index guide. These two regimes can be distinguished by the imaginary part of the eigenvalue, $\mathrm{Im}\,\mu$, i.e., by the modal gain per Rayleigh range z_0 [cf. Eq. (9)] or, equivalently, by the mirror reflectivity through $\mathrm{Im}\,\mu = -z_0 \ln R_m/2L$ [cf. Eq. (11)]. The parabolic index guide dominates when $\mathrm{Im}\,\mu \ll 1$, while the gain guide dominates when $\mathrm{Im}\,\mu \gg 1$.

These two regimes are illustrated in Fig. 2 for $w_g/w_0 = 0.30$, the case that will be studied in Sections 3 and 4. In Fig. 2 the guiding is shown in terms of the real and the imaginary part of the potential $V(\rho) = 2\rho^2 + z_0 g$ in Eq. (7), where $V(\rho)$ is proportional to Δn. The detuning was set at the point where the lowest threshold occurred; for comparison, the near-field intensity distribution of the lowest-loss eigenmode is also shown. The data are for $\mathrm{Im}\,\mu = 0.36$ and $\mathrm{Im}\,\mu = 6.3$ (corresponding to $R_m = 98\%$ and $R_m = 70\%$ in the experiment).

In the left-hand plot in Fig. 2 the real part of the refractive index is clearly dominated by the parabolic index guide. The gain-related index guide adds only a small extra dimple near the axis $\rho = 0$. Note that this corresponds to a small positive detuning in frequency [$\mathrm{Re}\,\Delta n_g > 0$ for $\Delta\omega > 0$; cf. Eqs. (5) and (6)], and a small additional focusing effect. Although the imaginary part of the refractive index is significant on axis, the lowest-loss mode extends beyond the radial range of the gain and is thus confined mainly by the parabolic index guide. Hence in this regime the index guide still dominates, as anticipated above.

For $\mathrm{Im}\,\mu = 6.3$, in the right-hand plot in Fig. 2, the gain-related guiding dominates. Both the real and the imaginary part of the gain-related guide are much stronger here (note the change in vertical scale with respect to the left-hand plot). The resulting decrease in width of the lowest-loss mode reduces the possible influence of the parabolic index guide even further. Note that the detuning is now even larger than in the left-hand plot, as can be seen from the increased relative strength of the gain-related index guide (in $\mathrm{Re}\,V$) compared with the pure gain guide (in $\mathrm{Im}\,V$). It may seem surprising at first that the lowest threshold is reached by detuning away from gain maximum. Although this detuning decreases the on-axis gain, the modal gain can still increase. This is because the additional gain-related index guide for positive detuning serves to further confine the eigenmode, improving the overlap with the gain function.

As noted in the introduction, in this paper we are particularly interested in the intermediate regime ($\mathrm{Im}\,\mu \approx 1$) where the parabolic index guide and the gain-related guiding are of similar strength. The experimental setup was specifically designed to address this regime.

3. EXPERIMENTAL SETUP

As was discussed in Ref. 13, the configuration shown in Fig. 1(a) can be mapped onto the configurations of Figs. 1(b) and 1(c), as long as the cavity length is shorter than the Rayleigh range of the cavity modes involved. Experimentally, the configuration of Fig. 1(c), consisting of a separate laser crystal and a concave mirror, is preferred, since it allows both flexibility and good control over the guiding parameters. For instance, the strength of the effective quadratic index guide is determined by the curvature of the concave mirror [cf. Eqs. (14)–(16) below and also the discussion in Section 5].

The cavity used in the experiments is shown in more detail in Fig. 3. The laser crystal is a 1% doped Nd:YVO_4 chip of 3 mm × 3 mm × 0.21(3) mm. The left face in the figure is coated antireflective at the pump wavelength, 808 nm, and highly reflective at the lasing wavelength, 1064 nm. The other face is coated antireflective at 1064 nm. An outcoupling mirror with a radius of curvature of $R_c = 200$ mm and a diameter of 10 mm is placed as close as possible to the latter end, leaving only a small air gap in between.

The distance between the laser crystal and the output coupler could be varied with a micrometer-based translation stage. In practice the two elements were first moved together until they touched at the edge of the crystal holder (diameter 5 mm) and then moved back a sufficient distance to allow fine alignment of the relative tilt. The resulting size of the air gap is estimated from the translation stage readout to be 0.10(3) mm, where the uncertainty is due mainly to variations in the precise alignment procedure.

The use of a separate output coupler allows us to switch output couplers, so that we can study the same cavity configuration with different outcoupling intensity reflectivities, i.e., different intracavity losses. Five different reflectivities R_m were used: 98%, 94%, 90%, 80%, and 70%. The laser crystal was mounted on a piezoelectric transducer, so that the cavity length could be fine-tuned on the subwavelength scale.

The microchip laser is pumped by a Coherent 899 titanium–sapphire laser operating at 808 nm. The titanium–sapphire laser itself is pumped by a Spectra-Physics Millennia laser operating at 532 nm. The transverse profile of the pump is Gaussian and has a waist size $w_g = 14\ \mu$m in the focus, on the crystal. The pump power incident upon the Nd:YVO_4 crystal was varied with a combination of a rotatable half-wave plate and a polarizer in the collimated part of the pump beam. Typical pump powers were in the 1–50 mW range.

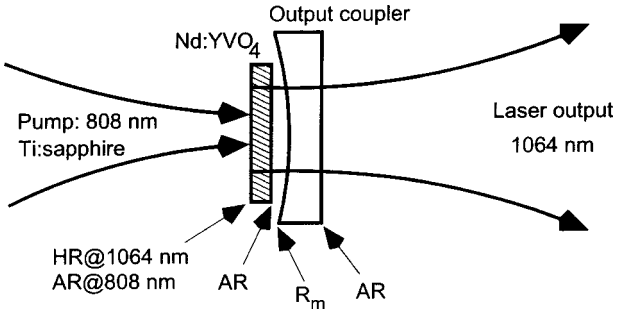

Fig. 3. Experimental setup of the microchip laser. The plano–concave configuration is longitudinally pumped by a titanium–sapphire laser at 808 nm. The crystal is ~200 μm thick with a refractive index of 2.2, and the air gap has a length of 0.1 mm. The radius of curvature of the output coupler is 200 mm. We can vary the reflectivity by replacing the output coupler with another one with the same radius of curvature.

The transverse profile of the output beam of the microchip laser was studied by alternately imaging the near field or the far field onto a HiSIS22 CCD camera with a calibrated two-lens imaging system. The estimated resolution of the imaging system was 3 μm for the near field and 0.2 mrad for the far field. Optical-quality beam splitters were used to reduce the intensity of the light incident upon the camera to within its dynamic range. The camera was custom modified by replacement of the original CCD device with a Kodak KAF-0440L CCD, which had an antiblooming system and (more important) which did not have a glass window in front of the chip. Avoiding this glass window eliminates optical interference effects originating from the reflection of the glass surfaces; this was found to significantly improve the quality of the images obtained. The size of the chip is 768 pixels × 512 pixels, where the physical size of one pixel is 9 μm × 9 μm; the camera is capable of producing 16-bit gray-scale images. The resulting mode profiles were generally found to have excellent circular symmetry. For comparison with the theoretical mode, a cross section was taken along the long (768-pixel) axis of the CCD chip through the center of the mode profile.

To map the experimental parameters for the configuration of Fig. 1(c) onto those of the theoretical model based on Fig. 1(a), we use Eqs. (12), (13), and (19) of our earlier paper.[13] For convenience these are reproduced here in the present notation, namely,

$$n_0 = \left[n_1 n_2 \left(\frac{n_1 L_1 + n_2 L_2}{n_2 L_1 + n_1 L_2} \right) \right]^{1/2}, \tag{14}$$

$$L = \left[\left(\frac{L_1}{n_1} + \frac{L_2}{n_2} \right) (n_1 L_1 + n_2 L_2) \right]^{1/2}, \tag{15}$$

$$w_0^2 = \frac{2}{k_z} \left(\frac{L R_c}{n_0} \right)^{1/2}. \tag{16}$$

An overview of all the relevant parameters of the laser used in the experiment is given in Table 1, including the model parameters derived by use of Eqs. (14)–(16). Note that the gain waist size w_g is indeed smaller than the waist size w_0 for the parabolic index guide, $w_g/w_0 = 0.30$.

The output of the laser was investigated spectrally by sending it through a planar Fabry–Perot interferometer. The laser was found to operate in a single transverse and longitudinal mode for all the data presented in Section 4. By operating the laser further above threshold, and carefully tuning the cavity length close to the point of a longitudinal mode hop, it was possible to have two longitudinal modes oscillating simultaneously. This allowed us to determine the longitudinal mode spacing to be 0.27(3) THz, where the estimated variation is due mainly to the fact that the cavity needed to be rebuilt for every different mirror reflectivity. This value is consistent with the the-

Table 1. Overview of the Experimental Parameters and the Corresponding Values of the Derived Theoretical Parameters

Variable	Description	Value
L_1	Crystal thickness	0.21(3) mm
n_1	Crystal refractive index	2.1652
L_2	Size of the air gap	0.10(3) mm
n_2	Refractive index of air gap	1
R_c	Mirror radius of curvature	200 mm
w_g	Gain (=pump) waist size	14(1) μm
λ_{at}	Laser output wavelength	1064 nm
γ_{at}/π	FWHM of the gain	207 GHz
L	Effective length	0.3 mm
n_0	Effective refractive index	1.7
w_0	Waist size of parabolic index guide	46 μm

oretical value based on the numbers in Table 1, $\omega_{FSR}/2\pi = c/2n_0L = 0.29$ THz. Note that the longitudinal mode spacing is somewhat larger than the gain bandwidth γ_{at}/π. This situation is typical for practical rare-earth microchip lasers and is favorable for single-mode operation.

In the case of the mirror with 90% reflectivity, it was also possible, under a very limited set of cavity and pumping conditions, to have two tranverse modes oscillating simultaneously. The estimated transverse-mode frequency splitting was 3(2) GHz, where the uncertainty is determined mainly by the difficulty of obtaining stable simultaneous oscillation in two transverse modes. This value is in rough agreement with the calculated value of 1.3 GHz.

4. RESULTS

A. Modal Thresholds

To compare the theoretical mode profiles with the experimental ones, it is necessary to know which of the modes will be lasing. Thus we first discuss in this section the modal thresholds, i.e., the pump power needed to bring each mode to threshold. We discuss the modal thresholds as a function of cavity detuning, and reflectivity. This also serves as a qualitative overview of the various regimes involved. In Subsection 4.B we then compare and discuss the theoretical and experimental transverse-mode profiles.

An overview of the threshold behavior as a function of cavity detuning is shown in Fig. 4. The left-hand side shows theoretical results, obtained through the methods described in Section 2 for the five different reflectivities used in the experiments. Each curve in the graphs represents the pump power needed to yield a particular mode at lasing threshold. Note that this value has been plotted such that the highest curve corresponds to the mode with the lowest lasing threshold. Each curve is smooth, and, when two curves cross, a different mode has the lowest threshold and will become the lasing mode. The lowest-loss transverse modes from adjacent longitudinal-mode manifolds [cf. Eq. (12)] have also been plotted to indicate the free spectral range. The right-hand side of Fig. 4 shows experimental results of the laser output power (i.e., *not* the threshold power) as a function of the cavity length. These were taken with the pump power fixed at a value close to the point where lasing over the entire free spectral range was just observed.

Although strictly speaking the left-hand and right-hand sides of Fig. 4 should not be directly compared, we do expect to see similar behaviors. When the laser is operated not too far above threshold, as in the experimental data of Fig. 4, the output power will usually be proportional to how far above threshold the laser is operated.[18] As long as the laser remains single mode (i.e., as long as the saturation is sufficiently homogeneous, both spatially and spectrally), we thus expect the experimental output power curve to follow the topmost curve of the calculated modal thresholds. A crossing of the theoretical curves should result in a discontinuous derivative of the experimental curve as the laser performs a mode hop (accompanied by a sudden change in transverse mode profile, as will be discussed extensively below).

Comparing the theoretical and experimental data in this way, we indeed see similar behaviors for each of the reflectivities. In addition, the modal behavior shows the signature of a transition from index-guiding dominated at high reflectivities to gain-guiding dominated at low reflectivities. At high reflectivity there are many modes with similar modal gains, but only the lowest-order modes (e.g., in the case of $R_m = 98\%$, the two modes shown in Fig. 4) have sufficient overlap with the localized gain to become the lowest-loss mode for a particular detuning.

For the lower reflectivities, Fig. 4 shows just a single smooth curve. In this case higher-order modes actually have much higher thresholds, and this reflects the strong mode discrimination that is typical for gain guiding.[13]

At intermediate reflectivities higher-order modes appear toward positive cavity-length detuning, each in a rather narrow range of cavity detunings. This effect is caused by the gain-related index guide and is discussed in more detail in Subsection 4.B. Figure 4 illustrates that the intermediate regime is of special interest: it exhibits features that are present neither in the index-guiding-dominated regime nor in the gain-guiding-dominated regime. Note also that in all cases the lowest threshold is achieved for a cavity detuning away from gain maximum toward a shorter cavity length, corresponding to $\Delta\omega > 0$, as was discussed for Fig. 2.

Apart from the general qualitative agreement between theory and experiment in Fig. 4, there are also quantitative differences. At 98% reflectivity the theory predicts two possible modes, but the experiment shows no discontinuities, just one mode. At 94% and 90% the theory also predicts more modes than the experiment shows (five versus three and six versus four, respectively). The modes that do not appear in the experiment are the last few higher-order modes in the calculations. This deviation and possible causes for it will be discussed more extensively in Section 5. We have verified that varying the theoretical parameters within the range allowed by experimental uncertainties is insufficient to resolve the discrepancy. The above comparison is possible only at positive cavity detunings where the higher-order modes appear. In contrast, it is almost impossible to determine

from Fig. 4 whether theory and experiment differ significantly for negative cavity detunings.

B. Modal Profiles

We now come to the main topic of this paper and compare the calculated and the experimental transverse modal profiles for each reflectivity. As a pragmatic solution to the systematic deviation between theory and experiment noted in Subsection 4.A, we have taken the following approach: for reflectivities of 98%, 94%, and 90% it was found that the profiles did not depend sensitively on cavity detuning (provided, of course that the detuning did not induce a mode hop). For these reflectivities we compare the experimentally observed modes with their theoretical counterparts for the cavity detuning that corresponds to the highest laser output and the lowest threshold.

For the lower reflectivities (80% and 70%) the modal profiles change continuously as a function of detuning. For large negative cavity-length detunings the modal profiles change only very modestly, but for small and positive detuning the changes are much more profound. Here we resort to a slightly different procedure for comparing theory and experiment, guided by the above observations. We assume that the most negative cavity detuning within the free spectral range in the theory and experiment match. Then we match the most positive cavity detuning within the free spectral range in the experiment to the largest detuning in the calculations for which the same high-order mode profile occurs as in the experiment (using the 94% and 90% reflectivity data). This leaves us with approximately 85(5)% of the original free spectral range in the theory to match with the entire free spectral range in the experiment. We note that this scaling is the only arbitrary scaling factor that we have applied to our data; all other theoretical parameters are directly taken from the experiment and have not been adjusted to improve the agreement between theory and experiment. Note also that a single set of values for the theoretical parameters was used to produce the full set of mode profiles discussed below.

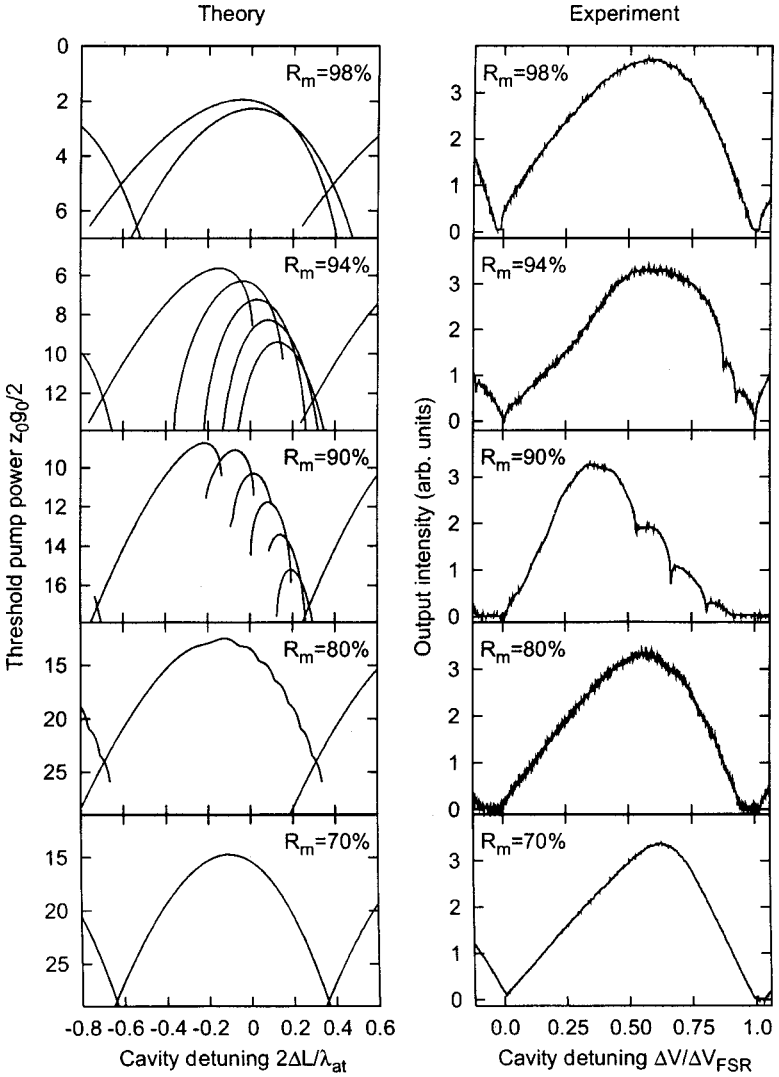

Fig. 4. Left, theoretical calculation of the threshold of the modes against the cavity detuning for various reflectivities of the outcoupling mirror. Right, experimental results that show the laser intensity output against the cavity detuning. The cavity detuning is measured in terms of the voltage ΔV on the piezo-electric transducer, normalized to the voltage required for scanning a full free spectral range ΔV_{FSR}. When in the calculation the laser jumps from one mode to the next, the experiment should show a small discontinuity as well.

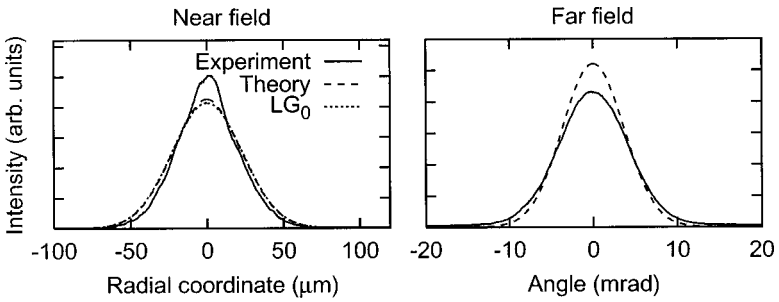

Fig. 5. Left, near-field and, right, far-field mode profile at reflectivity $R_m = 98\%$, for the cavity detuning corresponding to the lowest threshold. The solid curves are the experimental data, the dashed curves the result of the theoretical model. The index guide dominates (cf. Fig. 2), and the profile deviates very little from the profile of the lowest-order Laguerre–Gaussian mode LG_0 of the purely parabolic index guide (both in the near field and in the far field). The LG_0 mode is shown as the dotted curve in the near field; in the far field the LG_0 profile is not shown, as it would overlap the curve of the theoretical model.

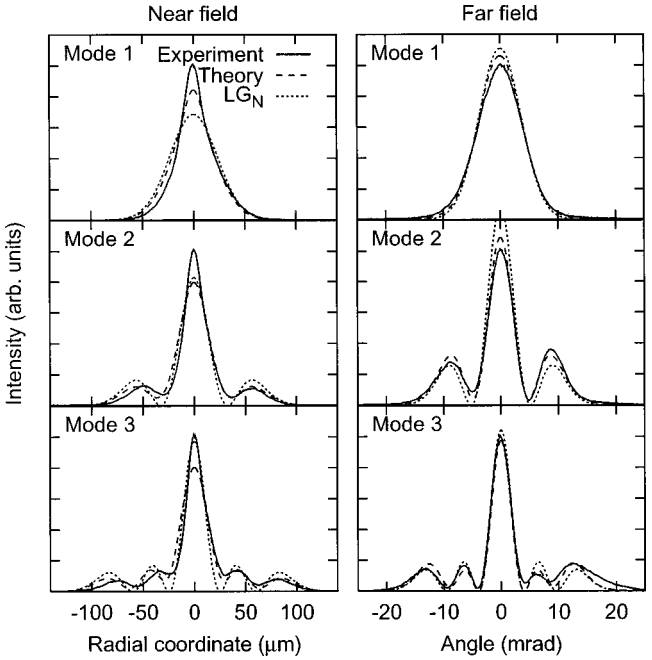

Fig. 6. Left, near-field and, right, far-field mode profiles at reflectivity $R_m = 94\%$. Three modes are found in the experiment (solid curves). These profiles match the results from the theoretical model (dashed curves) quite well. In contrast, both deviate from the three lowest-order Laguerre–Gaussian TEM modes of the parabolic index guide (LG_N, dotted curves); the near-field rings are weaker, and the far-field rings are stronger than those of the LG_N modes, and the intensity between rings does not go to zero.

For mirror reflectivity $R_m = 98\%$, we observe only one mode in the experiment. The modal profile changes very little as a function of detuning, both in the near field and in the far field. The theoretical and experimental profiles at the point of lowest threshold (highest output power) are compared in Fig. 5. The theory matches the experimental curve reasonably well, both in the near field and in the far field. For comparison the theoretical profile of the lowest-order Laguerre–Gaussian mode LG_0 of the purely quadratic index guide (Δn_R) is also shown. Clearly, the deviations from pure index guiding are rather small.

In Fig. 6 the three experimental mode profiles observed at $R_m = 94\%$ are compared with theoretical profiles. The three lowest-order Laguerre–Gaussian mode (LG_N, $N = 0,1,2$) of the pure parabolic index guide are also shown. Especially at the higher-order modes, there is a clear difference between LG_N on the one hand, where the minima go to zero, and our theory and experiment on the other, where the minima are nonzero. Note also that in the near field the additional rings are generally weaker than their LG counterparts, while in the far field the rings are generally stronger. These profiles can be interpreted as standard Laguerre–Gaussian profiles deformed under the influence of the gain guide.

For 90% reflectivity we have four modes, with four different profiles, shown in Fig. 7. Here the deviations from the conventional LG modes are obvious, as the direct comparison in Fig. 7 shows. The near-field patterns show only very weak rings, while in the far field the outer ring becomes quite strong—stronger in fact than the inner rings. In addition, the outer ring starts to merge with the inner rings. The theoretical mode profiles reproduce these features and match the experimental profiles quite well. The only significant difference is that the theoretical profiles seem to be more deeply modulated.

Based on the near-field profiles in Fig. 6 and Fig. 7, a qualitative explanation can now be given as to why each of these modes appears at a narrow range of detunings, a fact that was noted in Subsection 4.A; see Fig. 4. The near-field modal profiles are essentially strongly deformed Laguerre–Gaussians. Each mode has the lowest threshold when the overlap with the pump beam is maximized, i.e., when the rings are suppressed and when the central peak has a width similar to that of the gain profile, approximately one third of the LG_0 mode in Fig. 7. To deform the central peak in this way, the lowest-order mode, a deformed LG_0 mode, needs significant additional guiding. This additional guiding is provided by the gain-related index guide for positive detuning in frequency, i.e., for negative cavity-length detuning.

The next mode, a deformed LG_1 mode, requires less additional guiding, since the central peak of the LG_1 mode has a reduced width to begin with. The width of the central peak of the third mode, a deformed LG_2 mode, is similar to that of the gain profile; hence it does not need additional focusing, and it appears near zero detuning.[13] The central peak of the LG_3 and higher-order modes actually needs additional *antiguiding* for maximum overlap with the gain profile. Thus the related deformed modes will have the lowest threshold at negative frequency de-

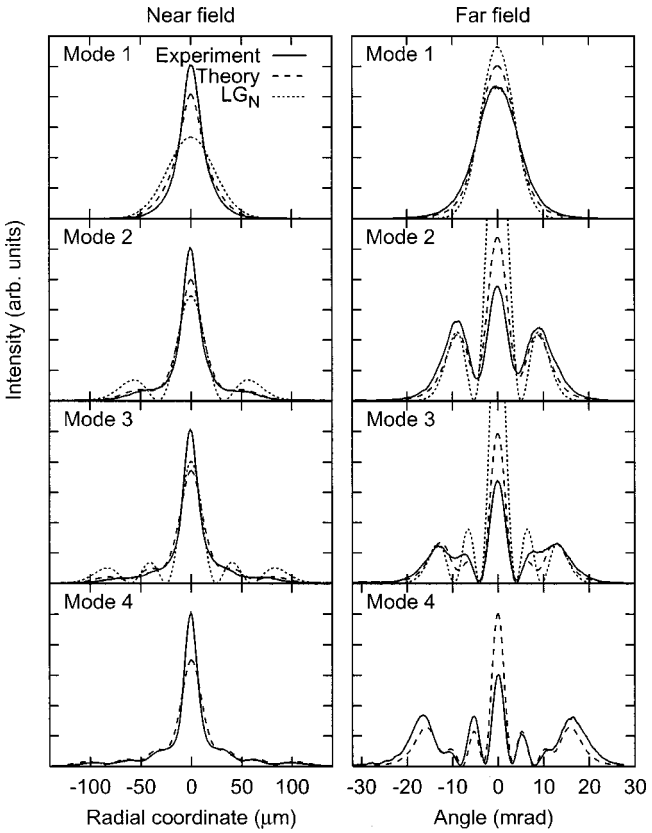

Fig. 7. Left, near-field and, right, far-field mode profiles at reflectivity $R_m = 90\%$. Four modes are found in the experiment (solid curves), and the profiles agree well with the results from the theoretical model (dashed curves), both in the near field and in the far field. For the higher-order modes the deviations from Laguerre–Gaussian modes are large: the near-field rings are strongly suppressed while the far-field rings become quite strong compared with the central peak. A direct comparison with the LG_N modes (dotted curves) is shown for the first three modes.

tuning (positive cavity-length detuning), where the gain-related index guide provides antiguiding. In summary, each deformed mode has a specific detuning at which the gain-related index guide yields maximum overlap with the gain profile. This effect is somewhat similar to mode pulling in a lossy cavity, the shift of the *longitudinal* modes toward the line center by the dispersion of the gain-related refractive index,[18] hence it could be called *transverse* mode pulling.

At 80% reflectivity we enter the gain-dominated regime, and only a single mode is observed (Fig. 8). In contrast to the above, however, the modal profile now does change shape, and it does so in a continuous fashion while the cavity is being detuned. The evolution of the near field is not very interesting, as it always shows a ringless profile, changing only in width when the cavity length is detuned. Note, however, that, since the profile is not Gaussian, the word "width" is actually ill-defined. Taking the standard deviation of such a profile as the width, we find that it decreases by approximately a factor of two when cavity lengths are detuned from short to long over the available free spectral range. Although a longer cavity length causes less focusing or even defocusing for the gain-related index guide, the mode also requires more on-axis gain to remain at threshold, causing the field to be pulled toward the center. Apparently, at longer cavity lengths the imaginary part of the gain guide has more influence on the mode formation than the gain-related index guide, causing a narrower near-field profile at longer cavity lengths.

The far-field profile changes much more dramatically. The continuously changing profile is illustrated by a number of representative examples in Fig. 8. The theoretical value for the cavity detuning $2\Delta L/\lambda_{at}$ is shown in the upper left corner of each graph (i.e., these numbers correspond to the horizontal axis in the left-hand part of Fig. 4). For negative cavity-length detunings the mode profile changes only slowly, while for positive cavity-length detunings the change is much more rapid.

Finally, at a mirror reflectivity of 70% the gain guide is even more dominant [see also Fig. 2(b)]. Again a single mode with a continuously changing profile as a function of detuning is observed. The shape in the near field seems to be fairly constant; it remains a more or less ringless profile (see Fig. 9). While detuning, again only the width of the profile changes.

The profiles in the far field, also shown in Fig. 9, are diverse. When detuning, we see the maximum intensity move outward continuously while new maxima and minima form in the center. This is an example of a laser showing conical emission.[10] This gives us profiles that

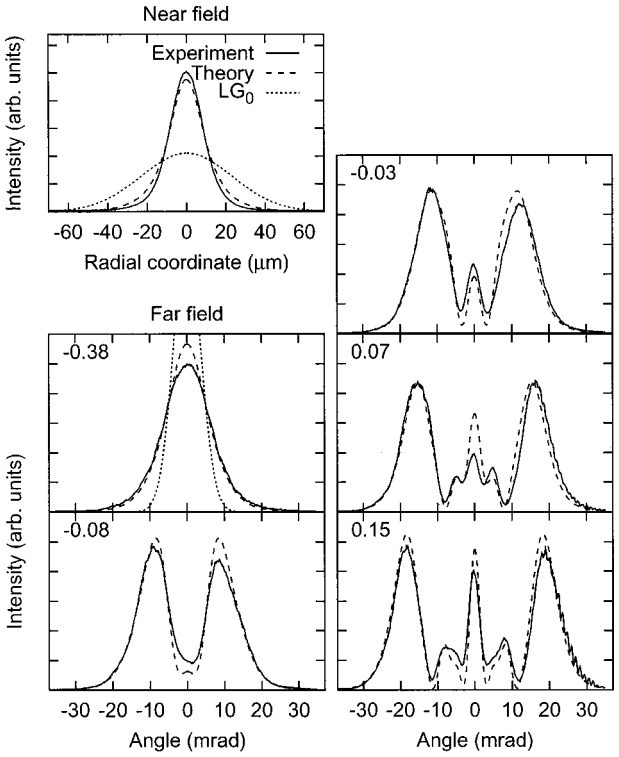

Fig. 8. Near-field and far-field profiles for $R_m = 80\%$ mirror reflectivity. The experimental data (solid curves) are again reproduced well by the theoretical model (dashed curves). The near-field profile changes only in width, and we show only one profile. The far-field profile changes much more drastically; a number of representative examples are shown. The value of the cavity detuning $2\Delta L/\lambda_{at}$ (cf. Fig. 4) of the theoretical curves is indicated in the graphs of the far-field profiles. The lowest-order Laguerre–Gaussian mode LG_0 of the purely parabolic index guide is also shown for comparison (dotted curves).

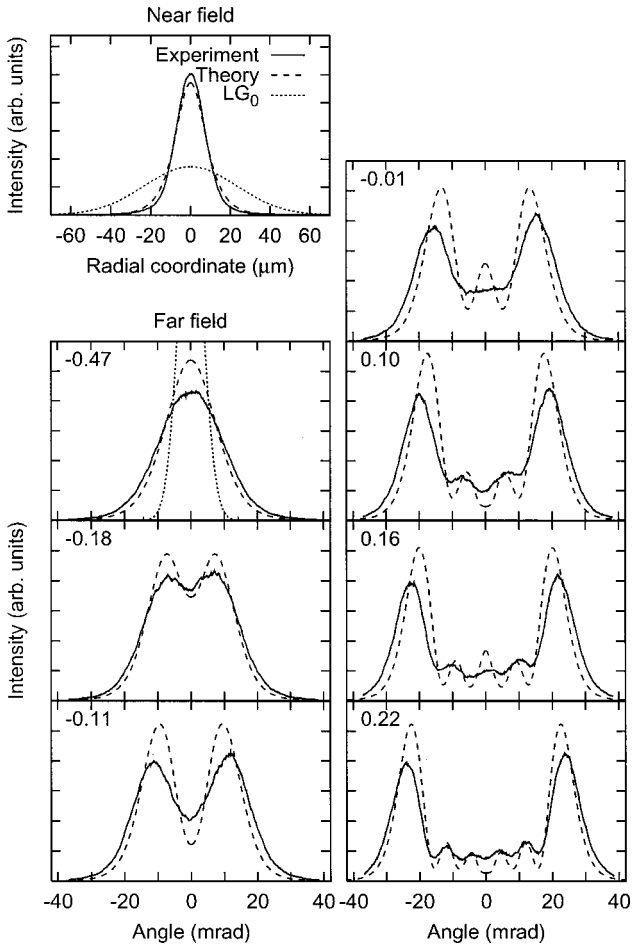

Fig. 9. Near-field and far-field profiles for mirror reflectivity $R_m = 70\%$. The gain guide dominates (cf. Fig. 2) and is stronger than for $R_m = 80\%$; the behavior shown in Fig. 8 becomes even more pronounced. The near-field profile changes only in width as the cavity detuning is changed, and only one example is shown. Representative examples of the far-field modal profiles illustrate how the maximum intensity moves off axis as the cavity detuning is changed. The value of the cavity detuning ($2\Delta L/\lambda_{at}$, cf. Fig. 4) is indicated for each far-field profile.

change from ringless to profiles with three rings. Note that the outer ring is the strongest and that the minima in the profile never go to zero. Also interesting is that the highest-gain profile in the far field has its maximum away from the center. Once again the agreement between theory and experiment is quite satisfying, considering the complexity of the observed behavior.

5. DISCUSSION

The agreement between the theoretical model and the experiments, as compared in Section 4, is surprisingly good. The large variety in observed modal profiles matches well with the model, which has essentially no adjustable parameters. The only serious discrepancy is in the range of accessible cavity detunings, which we have pragmatically removed with a single scaling factor.

For decreasing mirror reflectivity, the modal profiles show a transition from the usual Laguerre–Gaussian profiles for parabolic index guiding to profiles that are typical for gain guiding. For the lowest reflectivities our observations are similar to the predictions for a system with only the gain (-related) guiding of Longhi and Laporta:[10] in particular, we also find that the cavity detuning plays a major role and that conical emission appears for negative detuning in frequency. The similarities are striking, even though the actual transverse gain profile considered by Longhi and Laporta (a sech^2 function) is different from our (Gaussian) gain profile. In fact, the present study seems to be the first experimental demonstration of the kind of conical emission predicted by Longhi and Laporta. Apparently this behavior is a generic feature of gain guiding once the dispersive effect of the gain medium upon detuning from gain maximum (the gain-related index guide) is taken into account. As was already noted,[10] conical emission occurs when the gain-related index guide actually yields antiguiding (i.e., is equivalent to a negative lens, for negative detuning in frequency).

We now discuss the approximations made in the theoretical model and their relevance for the observed differences from the experimental data. The most important approximation we made in the theoretical model is describing the cavity as a longitudinally uniform waveguide; i.e., we have assumed that the gain medium, the gain, and the mirror curvature are spread throughout the cavity. For this to be a reasonable approximation, the transverse profile of the field inside the cavity must not change significantly during one round trip. To satisfy this requirement, the Rayleigh range of the field inside the cavity should be larger than the cavity length. However, since the transverse modal profiles are not really (Laguerre–) Gaussian, the Rayleigh range is not well defined. Instead it seems appropriate to use the waist size of the gain, $w_g = 14\,\mu$m, as the smallest near-field feature size expected (see also the curves for $R_m = 70\%$ in Fig. 2). This yields a lower boundary of $\sim$0.98 mm for the Rayleigh range, while the optical length of the cavity is $n_0 L = 0.51$ mm. Thus we expect the approximation to be reasonable but not perfect, and the observed size of the deviations (of the order of 10%) seems reasonable. We expect this to be the main cause of the observed deviations.

As further evidence for this conjecture, we mention here that we have done similar experiments for the same configuration (e.g., also with $w_g/w_0 \approx 0.3$) but with a more tightly curved mirror, $R_c = 25$ mm. In that case the Rayleigh range was approximately three times shorter, and the agreement between experiment and theory was significantly worse, in particular in terms of the number of observed modes.

We have also neglected all thermally induced guiding effects. It is possible that the heat deposited by the pump light causes an extra guide, but it will probably be weak compared with the two strong guiding mechanisms that we have included in the calculation. For instance, from a previous experiment[5] in which the thermal guiding alone was examined for a configuration similar to ours, the purely thermally guided mode would have a waist size of $\sim$200 μm. Since our mirror curvature alone gives much stronger guiding (the purely index-guided mode waist is 46 μm), we can assume that the thermally induced guiding effects are indeed negligible.

Another approximation in the theory is that we folded out the cavity to a waveguide, neglecting saturation. In the experiment, saturation can deform the transverse gain profile to be non-Gaussian through, for example, transverse spatial hole burning. Aside from this, the temporal dynamics, resulting from the slow inversion,[4] were neglected as well. Because of the slow inversion, the field inside the cavity fluctuates strongly in intensity near threshold. This fluctuation combined with the saturation might cause complicated forms of mode competition. It might cause higher-order modes to occur at, for example, higher cavity detunings. To avoid the effects of saturation as much as possible, the experiments were performed close to threshold (with a pump parameter of less than 1.3), and we may expect saturation effects on the transverse mode profiles to be relatively weak.

A last effect that might cause the gain profile to be deformed, probably resulting in less deeply modulated profiles, is the diffusion of excited states of the Nd^{3+} ions.[19,20] The typical diffusion length of an excited state (less than 0.5 μm), is ~4% of the waist size of the gain, and neglecting diffusion seems justified.

We now briefly discuss the effect of these results on common microchip lasers. The latter typically have a planar, monolithic design (whereas we have used an external concave mirror) and are operated far above threshold (whereas we have considered operation close to threshold). For a planar cavity the well-defined parabolic index guide of the concave mirror will be absent, and the index guide will be determined by thermal effects (thermal lensing and thermal curvature of the surface). Although the index guide will in principle have a nonparabolic shape, in practice approximating it as a parabolic index guide is often adequate[5] (as noted in Section 1). Thus our description should provide a good approximation.

A more quantitative comparison between microchip lasers and our experimental laser can be based on the rescaled Eq. (7), which contains as important dimensionless parameters the ratio w_g/w_0 of the pump beam size and the size of the eigenmode of the index profile, and the dimensionless gain per Rayleigh range $z_0 g_0$ (as well as the scaled frequency detuning $\Delta\omega/\gamma_{\mathrm{at}}$). The presented results are therefore directly applicable to microchip lasers, with their larger index-guided waist w_0, if the size of the pump spot is increased and if the mirror losses are reduced as compared with the values given in this paper; this is indeed the case in practical microchip lasers.

To describe a laser far above threshold requires a more significant extension of the present results. Far above threshold the effects of saturation of the gain medium need to be included in the theoretical description. The amount of saturation will depend on the local intensity.[6,8,11] As a result, the gain profile will depend on the intensity profile of the lasing mode and on how far above threshold the laser is operated. The gain profile will deviate from the pump profile and will generally become non-Gaussian. These complications are beyond the scope of this paper. The results presented here do provide a good starting point for further work in that direction. We expect that the essential features noted here (e.g., the role of the mirror reflectivity in determining the relative strength of the gain guide and index guide) will remain valid far above threshold.

6. SUMMARY AND CONCLUSIONS

In this paper we have theoretically and experimentally studied transverse-mode formation caused by combined Gaussian gain guiding and parabolic index guiding in a microchip laser. We have used a Nd:YVO_4 crystal and a separate curved mirror to form a plano–concave configuration pumped by a narrow-width Gaussian beam, resulting in the emission of an interestingly wide variety of transverse profiles.

We have shown that at higher reflectivities ($R_m \geqslant 90\%$ in our case), where we are still in the index-guide-dominated regime, higher-order modes appear with Laguerre–Gaussian-like profiles. The lowest-loss mode never has any rings, and the higher-order modes each have one ring more than the mode before; i.e., the laser profile is characteristic for the mode number. Also, with a decrease in reflectivity we see an increase in the number of visible modes. This is a consequence of the gain-related index guide, by means of transverse mode pulling. The deformation of the Laguerre–Gaussian profiles and the effects of the gain guide become stronger as well.

When lowering the reflectivity, there is a relatively sudden transition to the gain-dominated regime (in our case, for 80% and 70% reflectivity), and we see only one mode. The near-field profile is ringless, and changes only in width when the cavity is detuned. In contrast, in the far field the profile changes continuously. As the cavity length is increased, the maximum intensity moves outward; i.e., conical emission is observed, and rings appear inside. The more the cavity is detuned, the farther the high-intensity rings are from the center. This situation is typical for gain guiding, where a single trapped filament is supported with a smooth amplitude profile and a rapidly varying phase profile. This near-field phase structure leads to ring structure in the far field that strongly depends on detuning.

Theory and experiment show profiles with a similar number of rings, and these rings have similar strength. Also, the appearance of higher-order modes at high reflectivities and their disappearance at low reflectivities is reproduced by the theory. The deviations between theory and experiment are typically on the 10%–20% level. We expect that the approximation of the longitudinally uniform waveguide is the main source of these deviations. Going beyond this approximation would require a two-dimensional (radial and longitudinal) calculation, and hence a considerable additional computational effort. This is beyond the scope of this paper.

In conclusion, we have experimentally studied transverse mode formation in which several (anti)guiding effects are present, and we have used a relatively simple model for this intrinsically complicated process. Considering the simplifications made (as discussed in Section 5), we find excellent agreement between theory and experiment.

ACKNOWLEDGMENTS

The research of N. J. van Druten at Leiden University was made possible by the Koninklijke Nederlandse Akademie van Wetenschappen. We acknowledge support from the Foundation for Fundamental Research on Matter (FOM) and from the European Union under TMR Contract ERB4061PL95-1021 (Microlasers and Cavity QED).

*Present address, Department of Applied Physics, Delft University of Technology, Lorentzweg 1, 2628 CJ Delft, The Netherlands.

†Present address, Departament de Física i Enginyeria Nuclear, Universitat Politècnica de Catalunya, Escola Universitària d'Enginyeria Tècnica Industrial de Terrassa, Colom 1, 08222 Terrassa, Spain.

REFERENCES

1. J. J. Zayhowski and A. Mooradian, "Single-frequency microchip Nd lasers," Opt. Lett. **14**, 24–26 (1990).
2. J. J. Zayhowski, "*Q*-switched microchip lasers find real-world application," Laser Focus World **35**, August 1999, pp. 129–136).
3. C. Becher and K.-J. Boller, "Low-intensity-noise operation of Nd:YVO_4 microchip lasers by pump-noise suppression," J. Opt. Soc. Am. B **16**, 286–295 (1999).
4. N. J. van Druten, Y. Lien, C. Serrat, S. S. R. Oemrawsingh, M. P. van Exter, and J. P. Woerdman, "Laser with thresholdless intensity fluctuations," Phys. Rev. A **62**, 053808, 1–9 (2000).
5. J. J. Zayhowski, "Thermal guiding in microchip lasers," in *Advanced Solid-State Lasers*, H. P. Jenssen and G. Dubé, eds., OSA Proceedings Series **6** (Optical Society of America, Washington, D.C., 1991), pp. 9–13.
6. G. K. Harkness and W. J. Firth, "Transverse modes of microchip solid state lasers," J. Mod. Opt. **39**, 2023–2037 (1992).
7. T. Y. Fan, "Aperture guiding in quasi-three-level lasers," Opt. Lett. **19**, 554–556 (1994).
8. S. Longhi, "Theory of transverse modes in end-pumped microchip lasers," J. Opt. Soc. Am. B **11**, 1098–1107 (1994).
9. S. Longhi, G. Cerullo, S. Taccheo, V. Magni, and P. Laporta, "Experimental observation of transverse effects in microchip solid-state lasers," Appl. Phys. Lett. **65**, 3042–3044 (1994).
10. S. Longhi and P. Laporta, "Longitudinal-transverse mode interplay and conical emission in microchip lasers," J. Opt. Soc. Am. B **12**, 1511–1515 (1995).
11. F. Sanchez and A. Chardon, "Pump size optimization in microchip lasers," Opt. Commun. **136**, 405–409 (1997).
12. A. J. Kemp, R. S. Conroy, G. J. Friel, and B. D. Sinclair, "Guiding effects in Nd:YVO_4 microchip lasers operating well above threshold," IEEE J. Quantum Electron. **35**, 675–681 (1999).
13. C. Serrat, M. P. van Exter, N. J. van Druten, and J. P. Woerdman, "Transverse mode formation in microlasers by combined gain- and index-guiding," IEEE J. Quantum Electron. **35**, 1314–1321 (1999).
14. Y.-J. Cheng, C. G. Fanning, and A. E. Siegman, "Experimental observation of a large excess quantum noise factor in the linewidth of a laser oscillator having nonorthogonal modes," Phys. Rev. Lett. **77**, 627–630 (1996).
15. A. E. Siegman, "Excess spontaneous emission in non-Hermitian optical systems. I. Laser amplifiers," Phys. Rev. A **39**, 1253–1263 (1989).
16. A. E. Siegman, "Excess spontaneous emission in non-Hermitian optical systems. II. Laser oscillators," Phys. Rev. A **39**, 1264–1268 (1989).
17. M. P. van Exter, N. J. van Druten, A. M. van der Lee, S. M. Dutra, G. Nienhuis, and J. P. Woerdman, "Semi-classical dynamics of excess quantum noise," Phys. Rev. A **63**, 043801, 1–13 (2001).
18. A. E. Siegman, *Lasers* (University Science Books, Mill Valley, Calif., 1986).
19. H. G. Danielmeyer, "Effects of drift and diffusion of excited states on spatial hole burning and laser oscillation," J. Appl. Phys. **42**, 3125–3132 (1971).
20. J. J. Zayhowski, "The effects of spatial hole burning and energy diffusion on the single-mode operation of standing-wave lasers," IEEE J. Quantum Electron. **26**, 2052–2057 (1990).